Ignition Criteria for Trigger Waves in Cell Signaling

Brandon H. Schlomann [1,*] William S. DeWitt [2] Yuanzhao Zhang [3] and Kasturi Shah [4]

[1] *Department of Molecular and Cell Biology, University of California, Berkeley, California, USA*

[2] *Department of Genome Sciences, University of Washington, Seattle, Washington, USA*

[3] *Santa Fe Institute, Santa Fe, New Mexico, USA*

[4] *Department of Applied Mathematics and Theoretical Physics, University of Cambridge, United Kingdom*

(Received 22 August 2025; accepted 24 February 2026; published 6 April 2026)

To rapidly coordinate collective behaviors in tissues, cells communicate with one another through traveling fronts of signaling activity called trigger waves. The stimulus threshold for wave propagation is a key biological parameter that determines when the system produces a global response to a local stimulus. However, it is unclear how this stimulus threshold is determined by the properties of the underlying signaling network. To address this gap, we studied a model of trigger waves with a realistic Hill-type autoactivation function. We obtained an analytic expression for the wave ignition threshold in one dimension (1D) and numerical solutions in 2D and 3D. In the limit of high sensitivity, we found that the trigger wave threshold depends on both the effective dissociation constant, K_D, and the effective Hill coefficient, n, of the positive feedback circuit, with the dominant contribution scaling as $K_D^{n/(n-1)}$ in all dimensions. This result leads to a simple method for predicting the trigger wave ignition threshold from bulk activation data and is potentially of use for developing synthetic trigger wave circuits with desired sensitivities.

DOI: 10.1103/z7hq-1gxg

I. INTRODUCTION

Populations of cells signal to one another to coordinate collective behaviors. The secretion and diffusion of messenger molecules is a common mechanism of communication between cells [1] but is limited by the fundamental scaling of diffusive transport through the ambient fluid, $x \sim \sqrt{Dt}$, where x is space, t time, and D the diffusion coefficient [2]. For proteins in water, $D \approx 100\ \mu m^2/s$ [3], so diffusion over a cell length of approximately 10 μm occurs within a second, but diffusion across a centimeter-sized tissue takes days [4]. Thus, coordinating the activity of cells in tissues on faster timescales requires additional mechanisms.

One such mechanism is the ignition of signaling trigger waves [4]. Here traveling waves in the concentration of a signaling molecule (which can be proteins, ions, or other small molecules) are generated and travel across the system at constant speed, $x \sim ct$, enabling cell-cell communication on millimeter and larger length scales much faster than is possible by diffusion alone. Examples of trigger waves in cell signaling include waves of mitosis in developing embryos [5–7], calcium waves in response to wounds [8], waves in ERK signaling during tissue regeneration [9], and waves of coordinated cell death [10]. In addition, trigger waves have been predicted to occur in innate immune signaling pathways such as the TNF pathway [11,12].

Trigger waves arise from a combination of diffusion and positive feedback loops in signaling pathways that exhibit bistability [Fig. 1(a)]. Cells can exist in one of two stable states, marked by a low and a high concentration of an activating molecule. When one cell gets activated by a local stimulus, it secretes a molecule that diffuses toward and can activate the neighboring cell. If the stimulus is sufficiently strong, then each cell will activate its neighbor in a chain reaction, producing a traveling front [Fig. 1(b)]. When additional elements are added to the signaling pathway, such as negative feedback, more complex behaviors can arise, including transient pulses and oscillations [4]. A formula for the wave speed, deducible up to a prefactor from dimensional analysis, has been known for over a century [13] and provides a useful estimate for understanding the role of trigger waves in real systems [4]: $c = 2\sqrt{D/\tau_p}$, where D is the diffusion coefficient and τ_p is the timescale associated with the positive feedback.

Unlike the wave speed, how the stimulus threshold for wave ignition depends on the underlying biochemical signaling is much less well understood. This threshold is an important biological parameter, as it determines when the system produces a macroscopic, global response to a microscopic, local stimulus. Especially in contexts such as coordinated cell death [10] or immune activation [11], global activation of the tissue via a trigger wave has dramatic physiological consequences and so must be induced with care. At the same time, individual cells must retain some level of sensitivity in order to respond to local stimuli. How cells effectively tune their trigger wave activation threshold to achieve this balance is unclear. In addition, with continued advances in

*Contact author: bschloma@berkeley.edu

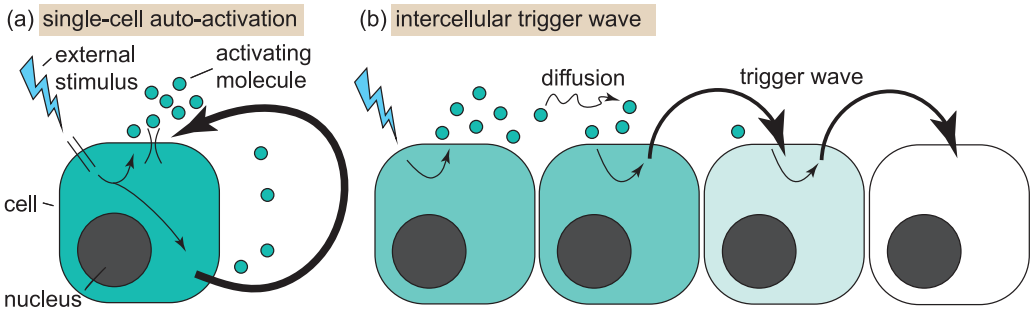

FIG. 1. Trigger waves in cell signaling arise from positive feedback and diffusion of secreted molecules. (a) Schematic of the positive feedback loop within single cells, which can be activated by an external signal. (b) Schematic of how a localized signal can excite a trigger wave that propagates across a tissue.

synthetic biology, there is increased interest in designing multicellular circuits that can be programed to perform specific functions in spatially structured environments such as tumors [14]. A better understanding of how to tune both cell- and tissue-scale sensitivities in bistable signaling networks is crucial for such efforts.

In this work, we study a minimal but biochemically relevant model of bistable trigger waves induced by a point source stimulus. This model represents tissues and organs subject to local stimuli such as a single infecting microbe, a single cell producing a chemical signal, a small wound, or activation of a synthetic biochemical circuit with optogenetics. Our work builds on previous works on analytic results for the trigger wave ignition criterion [15–21]. These previous studies focused on either general features of the activation threshold [15] or on models with analytically tractable autoactivation functions, especially of the cubic form [16–21]. Cubic functions capture the core behavior of trigger wave propagation, especially in the context of action potentials. However, it is difficult to map their parameters onto biochemical signaling networks, which are generally characterized by Hill-type activation functions [22,23]. Therefore, here we focus on a more realistic model with a Hill function governing autoactivation, at the expense of restricting our analysis to time-independent stimuli (see Appendix E for a detailed comparison of cubic and Hill models).

The model we investigate here is closely related to one that was recently studied numerically and was shown to describe trigger waves in reactive oxygen species involved in ferroptosis, a type of programed cell death [10]. Our model also represents a simplified version of inflammatory signaling via the cytokine TNFα, where the lack of negative feedback produces a state resembling "chronic inflammation" [11,12]. The bistable nature of the signaling dynamics we investigate here also have an ecological counterpart called the Allee effect, where a critical density of organisms is required to successfully reproduce [24]. More generally, our work contributes to a long-standing field of traveling waves in biological systems [24–32].

This paper is organized as follows. First, we introduce our partial differential equation (PDE) model and establish some of its basic properties. Second, to gain intuition, we study the threshold behavior of a simplified ordinary differential equation (ODE) model that describes the average behavior of a well-mixed population of cells subject to a uniform stimulus. This model represents experiments in which cells are activated in bulk within a stirred flask. Third, we study the full model and compute the critical stimulus threshold required to activate a spatially extended population of cells with a localized stimulus, analytically in the one-dimensional version of our model and numerically in the two- and three-dimensional versions. We find that in all spatial dimensions the activation threshold scales the same way with the dissociation constant of the autoactivation circuit. This result leads to a simple method for predicting the trigger wave ignition threshold from straightforward measurements of bulk activation in well-mixed environments, which may be useful for understanding when to expect trigger waves to occur in natural and synthetic signaling systems. As an example of such an analysis, we applied our results to the inflammatory cytokine TNFα. Though trigger waves in the concentration of this molecule have been predicted to occur on theoretical grounds, experiments have yet to observe such waves, despite this system exhibiting rich spatiotemporal behavior [33]. Our results suggest that the stimulus threshold for wave ignition may be higher than is experimentally accessible, offering a possible explanation for why traveling waves have not yet been observed in this system.

II. RESULTS

A. Model definition and basic properties

We begin by considering a reaction-diffusion system describing the concentration of an activating molecule, $u(\vec{x}, t)$, on a d-dimensional lattice containing many cells [Fig. 2(a)]. We model a generic autoactivating signaling network by combining an effective Hill function describing the positive feedback loop with a first-order decay process [10,22,34] coupled in space by diffusion. We consider subjecting one cell, located at the origin, to a localized stimulus with rate $2I$ (units of amount of u per time; the factor of 2 is conventional [19]). Putting these ingredients together and taking the continuum limit, we obtain

$$\partial_t u = D\nabla^2 u + k\frac{u^n}{K_D^n + u^n} - \gamma u + 2\,(l_{\text{cell}})^d\, I\,\delta(\vec{x}). \quad (1)$$

Here D is the diffusion coefficient, k is the maximum production rate, n is the Hill coefficient that sets the sharpness of the autoactivation circuit, K_D is the effective dissociation constant that sets the sensitivity of the autoactivation circuit

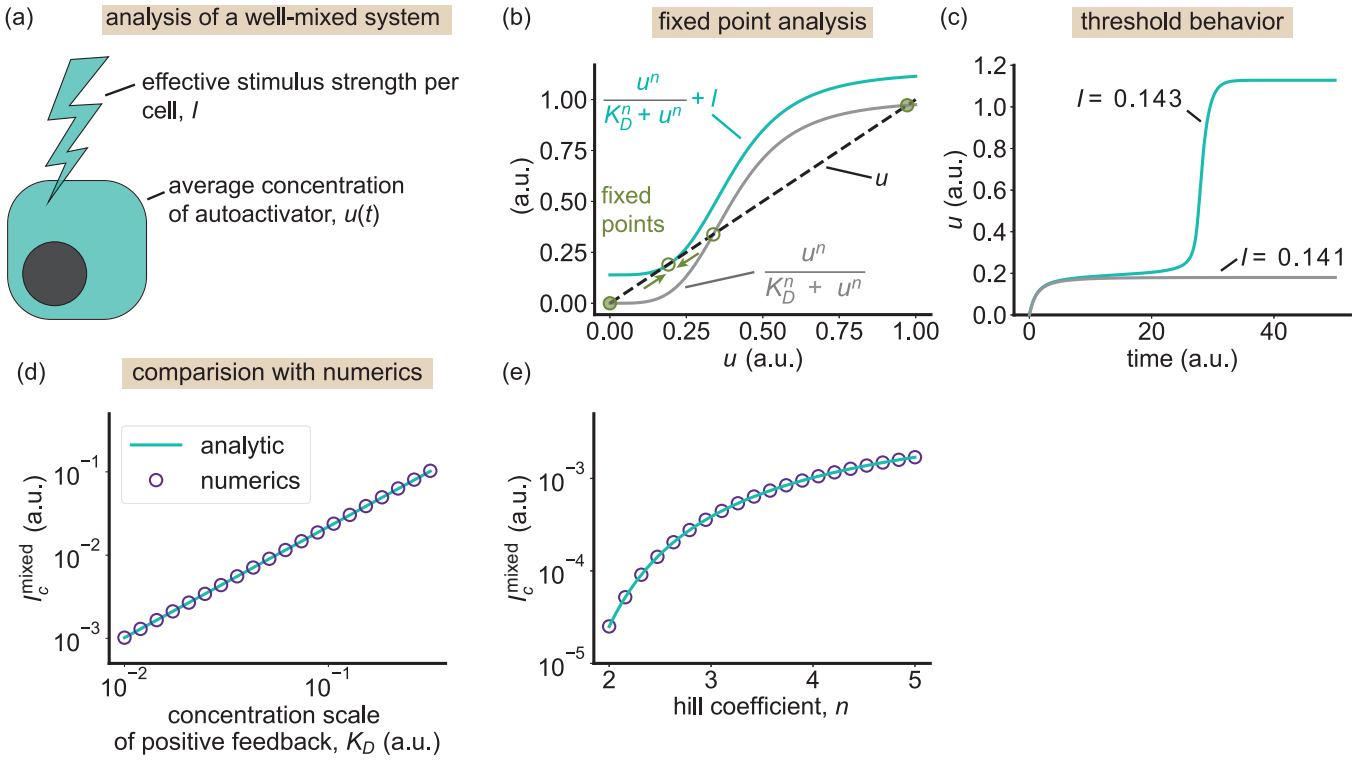

FIG. 2. Analytic results for well-mixed activation agrees well with simulation. (a) Schematic of the well-mixed problem. Assuming uniform stimulation and fast mixing (e.g., a stirred flask), we can ignore diffusion in Eq. (1) and analyze the ODE in Eq. (6) for the average response driven by an effective stimulus strength per cell, written here schematically as I; see Eq. (6) for details. We seek the critical value of I that activates the system into its high stable state. (b) The key idea of our calculation is to study the fixed point structure of the activation function, $f(u)$. Beyond a critical value of the stimulus strength, the system will lose its low stable fixed point and $u(t)$ will always go to the activated high state. The fixed points of $f(u)$ are shown in green (stable points filled). (c) Example response for I below (gray line) and above (cyan line) the critical threshold. [(d) and (e)] Comparison between the analytical and numerical results for the critical threshold, I_c^{mixed}, as a function of model parameters. Parameters: in (d), $n = 4$ and in (e), $K_D = 0.01$.

(it is the concentration of u at which the positive feedback becomes relevant), and γ is the loss rate, which can be due to degradation or absorption. The effective Hill function parameters, n and K_D, describe the response of the full signaling network—which may include many intermediate steps—to autoactivation and can in principle be determined empirically by exogenously varying the concentration of the activator and measuring the response. The localized stimulus at the origin is described by the Dirac delta function, $\delta(\vec{x})$, with the prefactor $(l_{\text{cell}})^d$ representing the lattice voxel (see Appendix A for details; keeping track of lattice size is useful for our comparison to the nonspatial model in Sec. II B). We restrict our analysis to parameter regimes where the model locally exhibits bistability, with low-u and high-u stable states.

Our goal is to calculate the critical threshold, I_c^{wave}, that will trigger a traveling wave solution in Eq. (1) and to understand how different biochemical parameters influence the trigger wave threshold. To simplify the analysis, we nondimensionalize Eq. (1) via $u \to u/(k/\gamma)$, $t \to \gamma t$, $\vec{x} \to \vec{x}/\sqrt{D/\gamma}$. The resulting dimensionless governing equation is

$$\partial_t u = \nabla^2 u + \frac{u^n}{K_D^n + u^n} - u + 2\,(l_{\text{cell}})^d\, I\, \delta(\vec{x}), \tag{2}$$

where K_D and $(l_{\text{cell}})^d I$ have been rescaled appropriately. This model only has three parameters: the dimensionless dissociation constant, K_D, the Hill coefficient, n, and the dimensionless stimulus strength, $(l_{\text{cell}})^d I$. We also define the activation function

$$f(u) := \frac{u^n}{K_D^n + u^n} - u \tag{3}$$

and its three fixed points, $u_1 < u_2 < u_3$.

As we will see below, the structure of $f(u)$ and the values of its fixed points—especially u_2—determine much of the behavior of Eq. (1). Therefore, we calculate them here by setting $f(u) = 0$ and solving for u. The low activity state is trivially $u_1 = 0$. To make analytic progress on u_2 we work in the limit $K_D \ll 1$. This approximation corresponds to a limit of high sensitivity, where the concentration scale of u that induces positive feedback is small compared to the equilibrium value of u in the high state. This approximation is reasonable because K_D generally must be small (<1) for the system to be bistable. The intermediate fixed point, u_2, satisfies

$$u_2^{n-1} - u_2^n = K_D^n. \tag{4}$$

Since u_2 is set by K_D, which we take to be small, we conjecture that u_2 is also small and will check this conjecture with

a posteriori reasoning. Assuming that u_2 is small, we can neglect the u_2^n term and find that

$$u_2 \approx K_D^{\frac{n}{n-1}} \tag{5}$$

plus higher-order terms, which are indeed small for $n > 1$. By similar reasoning, the high fixed point, u_3, is given by $u_3 \approx 1 - K_D^n$ for $K_D \ll 1$. With these fixed points computed, we can begin to understand the behavior of Eq. (1).

B. Well-mixed analysis

To gain intuition about how the Hill function parameters, K_D and n, control the nonlinear response of the system, we begin by studying the mean-field behavior of Eq. (1), describing the average response of a well-mixed population of cells [Fig. 2(a)]. To do this, we consider the ODE counterpart to Eq. (1),

$$\dot{u} = k\frac{u^n}{K_D^n + u^n} - \gamma u + 2I. \tag{6}$$

Here all cells are subject to the same driving stimulus of strength $2I$ [units of amount of u per time; defining I as we did for Eq. (1), with the factor of l_{cell} scaled out, allows us to directly compare the spatially dependent and nonspatial models]. For this system, the critical stimulus threshold for activation, I_c^{mixed}, corresponds to the value of I that eliminates the low-u stable fixed point in Eq. (6) [Figs. 2(b) and 2(c); Appendix B]. In the low-K_D limit, we use a result for the discriminant of a special set of nth-order polynomials [35] to compute this threshold to be

$$I_c^{\text{mixed}} = \frac{1}{2}\left(1 - \frac{1}{n}\right)\left(\frac{1}{n}\right)^{\frac{1}{n-1}} K_D^{\frac{n}{n-1}}, \tag{7}$$

or, in dimensionful units,

$$I_c^{\text{mixed}} = \frac{1}{2}\left(1 - \frac{1}{n}\right)\left(\frac{1}{n}\right)^{\frac{1}{n-1}}\left(\frac{K_D}{k/\gamma}\right)^{\frac{n}{n-1}} k \tag{8}$$

(see Appendix B for details). This result agrees well with simulations over a wide range of parameters [Figs. 2(d) and 2(e)]. Intuitively, this result tells us that decreasing the sensitivity (increasing K_D) and increasing the sharpness (increasing n) of the autoactivation circuit make it harder to activate the system.

The key takeaway from our result is the scaling of the stimulus threshold with $K_D^{n/(n-1)}$, which describes how the dissociation constant, K_D, and the Hill coefficient, n, of the autoactivation pathway combine to determine the nonlinear response of the system. It is interesting to note that the stimulus threshold inherits its dependence on K_D from the intermediate fixed point of the activation function, u_2 [Eq. (5)]. We next seek to understand if this mean-field behavior also controls the ignition of trigger waves in spatially extended systems.

C. Trigger wave ignition threshold

To compute the wave ignition threshold [Fig. 3(a)] in $d = 1$, we follow the approach of Mornev [15] (recently introduced to a wider audience in Ref. [21] and also related to approaches outlined in Ref. [36]), which applies to arbitrary activation functions with time-independent stimuli in one dimension. This approach exploits the mapping between stationary solutions of one-dimensional reaction diffusion systems and the dynamics of a single-particle Hamiltonian system [36]. The idea is to identify for what values of I do steady-state solutions of Eq. (1) that decay to zero at infinity, $u(x \to \pm\infty) = u'(x \to \pm\infty) = 0$, cease to exist. In Appendix C, we show that such decaying steady-state solutions are constrained by the following relationship between $u(x)$ and its derivative, $u'(x) = \partial_x u$:

$$u' = \left(-2\int du\, f(u)\right)^{1/2}. \tag{9}$$

Drawing this solution set in the u-u' plane, we see that it forms a closed curve that starts and ends at $(0, 0)$ [Fig. 3(b), gray curve]. Traveling along this curve clockwise outlines the shape of a localized steady-state profile [Fig. 3(c)]. In contrast, solutions with spatially uniform activation contain the point $(u, u') = (u_3, 0)$, with u_3 the high fixed point of $f(u)$ and $u' = 0$ describing a flat activation profile; this solution set is drawn in Fig. 3(b) as a cyan curve (see Appendix C for details).

Since the delta function stimulus in Eq. (1) fixes the value of u' at $x = 0$, we can draw this boundary condition as a pair of horizontal lines in the u-u' plane [one for $\lim_{x\to 0^+}$ and one for $\lim_{x\to 0^-}$; Fig. 3(b), dashed black lines]. As I increases, these horizontal lines move away from the x axis. The critical stimulus strength to ignite a wave, I_c^{wave}, corresponds to the point at which these horizontal lines lift off of the lower solution branch [indicated by black arrows in Fig. 3(b); this transition is shown in Figs. 3(c) and 3(d)]. It can be shown that this point—which corresponds to the apex of the lower branch—occurs at $u = u_2$, the intermediate, unstable fixed point of $f(u)$ (see Appendix C) [15]. Therefore, I_c^{wave} can be computed by solving the integral

$$l_{\text{cell}} I_c^{\text{wave}} = \left(-2\int_0^{u_2} du\, f(u)\right)^{1/2}. \tag{10}$$

We solved this integral to leading order in the limit $K_D \ll 1$, corresponding to a high-sensitivity limit (Appendix C). We find the trigger wave threshold to be

$$l_{\text{cell}} I_c^{\text{wave}} = \left(\frac{n-1}{n+1}\right)^{1/2} K_D^{\frac{n}{n-1}}, \tag{11}$$

or, in dimensionful units,

$$I_c^{\text{wave}} = \left(\frac{n-1}{n+1}\right)^{1/2}\left(\frac{K_D}{k/\gamma}\right)^{\frac{n}{n-1}}\left(\frac{D}{\gamma\, l_{\text{cell}}^2}\right)^{1/2} k. \tag{12}$$

This result agrees well with numerical simulations across a wide range of parameters [Figs. 3(e) and 3(f)]; see Appendix F for our numerical scheme. The key insight from this result is that the stimulus threshold for wave propagation scales with K_D in same way as the activation threshold for well-mixed systems [Eq. (7)], namely scaling as $K_D^{n/(n-1)}$. This identical scaling behavior leads to some interesting consequences for experiments that we elaborate below. Before exploring these consequences, however, we check if this result is robust to modifications of the model in terms of its dynamics and spatial dimension.

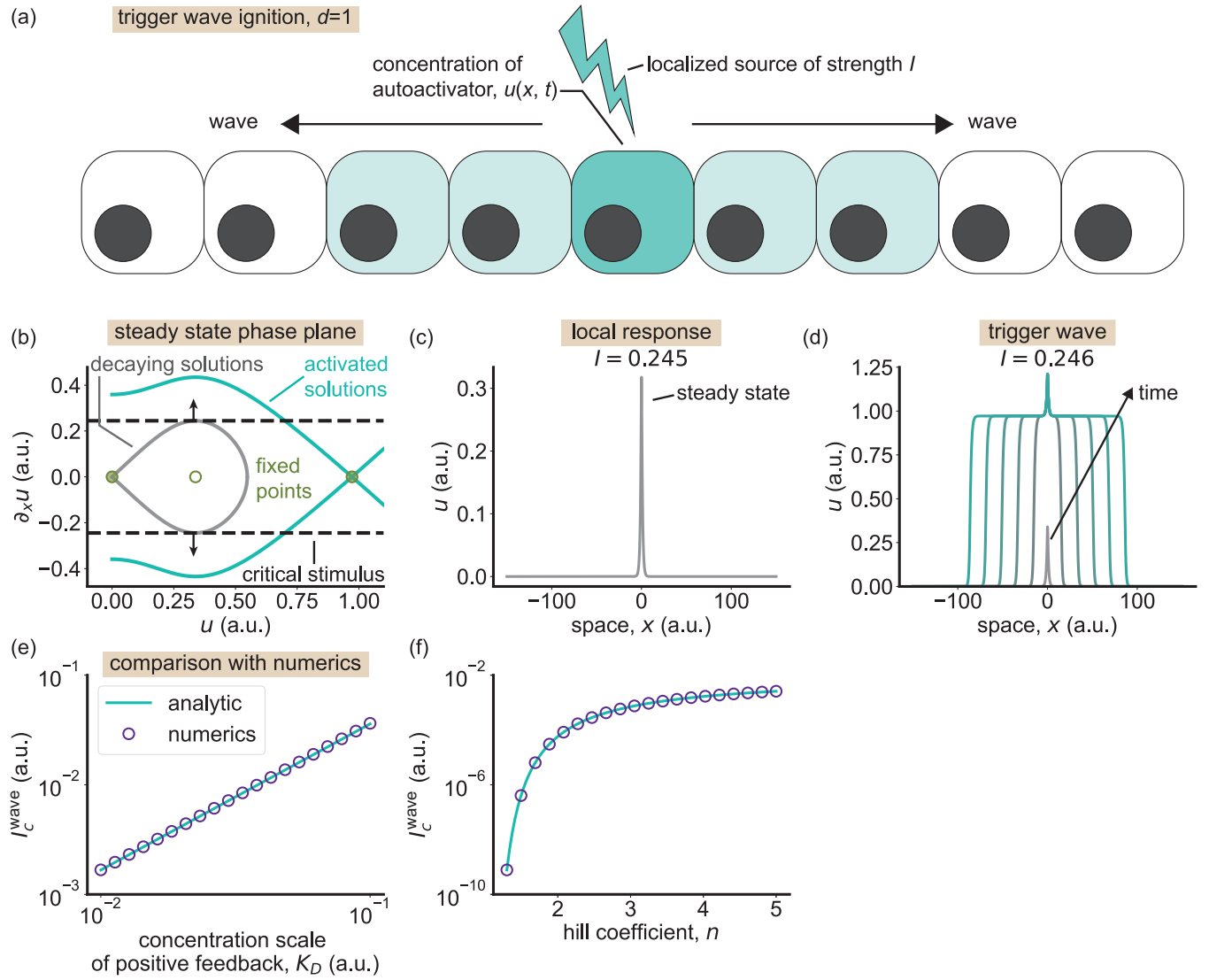

FIG. 3. Analytic result for trigger wave ignition criteria agrees well with simulation. (a) Schematic of the spatially extended problem. We consider a 1D grid of cells that produce and consume an autoactivating molecule, $u(x,t)$. One cell at the origin is subjected to a constant stimulus of strength I. We seek the critical value of I that ignites a wave of u activity. (b) The idea of the calculation is to study the existence of steady-state solutions in the u-u' plane. Solutions that decay in space, with $u(x \to \pm\infty) = u'(x \to \pm\infty) = 0$ lie on the solid gray line. Solutions that are uniformly high in the activated state lie on the solid cyan line. The boundary conditions on $u'(x = 0^{\pm})$ are shown as horizontal black dashed lines. Beyond a critical value of the stimulus strength, I, the boundary condition at the origin can only be satisfied by the cyan (activated) solution set, corresponding to the onset of trigger waves. The three fixed points, $u_1 < u_2 < u_3$, of the activation function, $f(u)$, are shown in green (stable points filled). The critical stimulus value corresponds to the point $u'(u_2)$ on the gray (decaying) solution set. (c) Example of a local steady-state response for I below the critical threshold. (d) Example of a trigger wave response above the critical threshold. [(e) and (f)] Comparison between the analytic and numerical results for the critical threshold, I_c^{wave}, as a function of model parameters (l_{cell} absorbed into the definition of I). For (e) $n = 4$ and for (f), $K_D = 0.01$.

Since positive feedback in real signaling circuits does not happen instantaneously, but is often mediated through slow intermediate molecules, we expanded our model to include such a time delay by coupling the production of u to a second, slow variable (Appendix D). In this model, the slow intermediate variable could represent, for instance, the localization of a transcription factor to the nucleus [37]. We found that the scaling of the ignition threshold with K_D holds true in models with a time delay, with only the prefactor growing as the delay gets longer (Appendix D). Therefore, we conclude that the scaling behavior $I_c^{\text{wave}} \sim K_D^{n/(n-1)}$ is robust to the inclusion of delayed autoactivation.

To understand how our result for I_c^{wave}, obtained analytically for $d = 1$ in the limit $K_D \ll 1$, changes in higher spatial dimensions, we performed numerical simulations. We found numerically that the same scaling behavior, $I_c^{\text{wave}} \sim K_D^{n/(n-1)}$, also occurs for $d = 2$ and $d = 3$ [Fig. 4(a); some noticeable deviation occurs for $d = 3$ at larger K_D, indicating that the small K_D approximation breaks down sooner here]. This empirical observation suggests that the wave ignition threshold

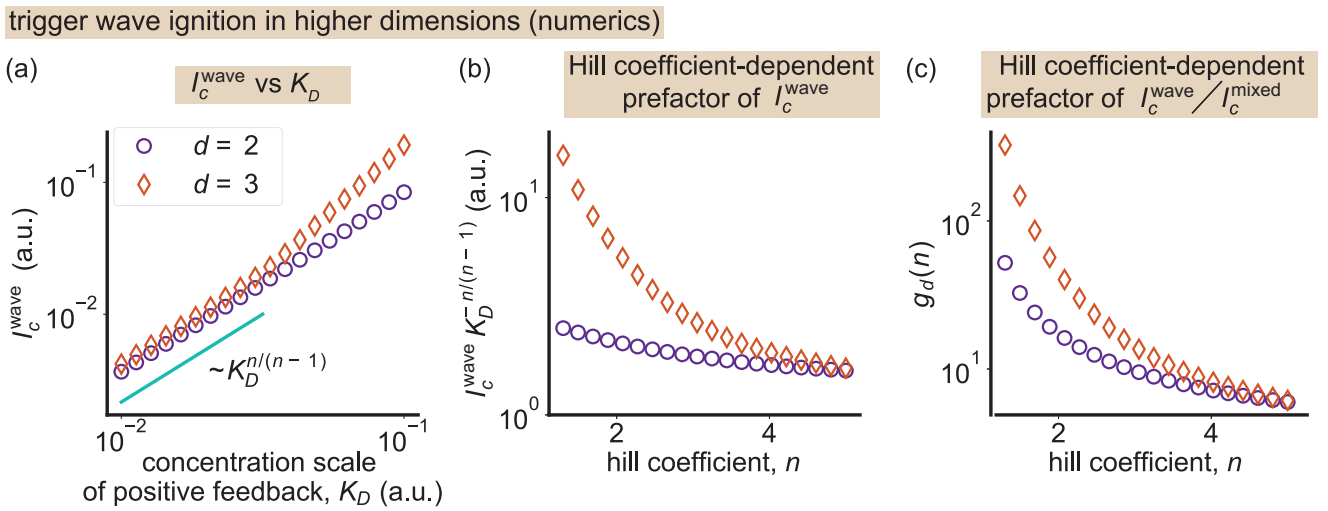

FIG. 4. The scaling of the trigger wave threshold with K_D extends to higher dimensions. (a) Comparison between the scaling prediction of the critical threshold, I_c^{wave}, as a function of K_D for $d = 2$ (purple circles) and $d = 3$ (orange diamonds; l_{cell} is absorbed into the definition of I). The scaling behavior seen in the well-mixed system and in $d = 1$ (cyan line) holds in higher dimensions for $K_D \ll 1$. (b) Numerical results for the Hill coefficient-dependent prefactor of I_c^{wave}. (c) Numerical results for the Hill coefficient-dependent prefactor of $I_c^{\text{wave}}/I_c^{\text{mixed}}$, defined as $g_d(n)$ in Eq. (14). For (a) $n = 4$ and for (b) and (c), $K_D = 0.01$.

can be written in a universal form for all spatial dimensions:

$$I_c^{\text{wave}} \sim \left(\frac{K_D}{k/\gamma}\right)^{\frac{n}{n-1}} \left(\frac{D}{\gamma\, l_{\text{cell}}^2}\right)^{d/2} k, \tag{13}$$

for $K_D/(k/\gamma) \ll 1$. In this expression, the K_D term is our proposed heuristic based on our analytic results in $d = 1$ [Eq. (11)] and our numerical simulations for higher dimensions [Fig. 4(a)]. The rest of the terms follow directly from dimensional analysis. To validate our dimensional analysis, we obtained numerical solutions of the dimensionful model in Eq. (1) and computed how I_c^{wave} depends on the diffusion coefficient, D (Appendix F). We find excellent agreement with theory $I_c^{\text{wave}} \sim D^{d/2}$ in all spatial dimensions, indicating that Eq. (13) provides a useful summary of the the trigger wave threshold over a wide range of parameters.

An interesting consequence of this scaling behavior is that the ratio between the wave and well-mixed thresholds can be written in a surprisingly simple form,

$$\frac{I_c^{\text{wave}}}{I_c^{\text{mixed}}} = g_d(n)\left(\frac{l_D}{l_{\text{cell}}}\right)^d, \tag{14}$$

where $g_d(n)$ contains the dependence on the Hill coefficient, $l_D = \sqrt{D/\gamma}$ is the diffusive length scale, and l_{cell} is the size of a cell. In $d = 1$, the Hill coefficient-dependent prefactor to the wave:mixed threshold ratio, $g_d(n)$, is given by

$$g_1(n) = \frac{2\left(\frac{n-1}{n+1}\right)^{1/2}}{\left(1-\frac{1}{n}\right)\left(\frac{1}{n}\right)^{\frac{1}{n-1}}}, \tag{15}$$

which is a decreasing function of n for which $g_1(2) \approx 4.62$ and $g_1(\infty) = 2$. In higher dimensions, we find numerically that there is a larger dynamic range of the Hill coefficient-dependent prefactor of I_c^{wave} [Fig. 4(b)], which translates to a larger dynamic range of $g_d(n)$ [Fig. 4(c)]. We find that $g_d(n = 4) \approx 7$ in $d = 2$ and $d = 3$ but takes on larger values at smaller n with $g_2(2) \approx 16$ and $g_3(2) \approx 48$. However, in most of parameter space, the dominant contribution to the trigger-wave-to-bulk activation ratio comes from the ratio of diffusive to cellular length scales. As we discuss below, this result suggests a simple method for predicting the ignition threshold of a trigger wave circuit based on straightforward bulk measurements of cellular activity.

III. DISCUSSION

In this paper, we studied a reaction-diffusion model of cell signaling trigger waves governed by a Hill function-based autoactivation circuit. When this model is bistable, its behavior is qualitatively similar to the well-studied Nagumo equation, $\partial_t u = \partial_x^2 u + u(u-\theta)(1-u)$ [19]. The cubic form of the activation function in the Nagumo equation has enabled a wealth of analytic results, including detailed analysis of time-dependent stimuli [19,21]. However, in the context of cell signaling trigger waves, autoactivation circuits are characterized by Hill functions not cubic functions. The key difference between the two is that Hill functions can support higher degrees of nonlinearity than cubic polynomials [22,23] and also saturate at high input levels. Our contribution in this paper is to understand the quantitative details of how the wave ignition threshold depends on Hill function parameters—the sensitivity, K_D, and the sharpness, n—that describe real biochemical signaling networks [22,23].

Our results have some practical implications for experiments. The ratio of the wave to well-mixed activation thresholds is a simple function whose value is set primarily by the ratio of diffusive to cellular length scales, $l_D/l_{\text{cell}} = \sqrt{D/\gamma}/l_{\text{cell}}$. Therefore, if one measures the activation threshold in bulk with a population of cells, for example by flow cytometry [38], then one can make a prediction for the trigger wave ignition threshold simply by knowing the diffusion coefficient and half-life of the signaling molecule. This simple estimate could be useful for understanding when we should expect to see trigger waves occur in tissues.

For example, trigger waves of the proinflammatory molecule TNFα have been predicted to occur based on the topology of its signaling pathway and measured parameter values [11,12]. However, despite exhibiting rich spatiotemporal dynamics [33], trigger waves of TNFα have not yet been observed experimentally (some suggestive evidence in a similar pathway in fruit flies does exist [39]). One possibility is that, while the TNF pathway exhibits positive feedback, it may not have parameter values that support traveling wave solutions. However, another possibility is that the stimulus threshold to ignite the wave is higher than stimulus levels that have been tested experimentally. Using a typical value for a signaling protein diffusion coefficient, $D = 100\ \mu m^2/s$, an experimentally measured loss rate of $\gamma = 3 \times 10^{-3}\ s^{-1}$ (half-life of $\approx$5 min, due primarily to absorption by cells [40,41]), and a cell size of 10 μm, we have that the ratio of diffusive to cellular length scales is approximately 18. Therefore, as a lower bound, we predict that the trigger wave threshold is at least 18 times that of the well-mixed activation threshold in $d = 1$. This value is comparable to the approximate value of 10 reported in Ref. [11] for a more detailed simulation of TNF signaling, suggesting that our simplified model captures the correct order of magnitude of the threshold behavior in this system. For higher dimensions, this lower bound on the activation threshold ratio becomes 324 in $d = 2$ and approximately 5800 in $d = 3$. Since the stimulus strength, I, can be interpreted as the initial rate of autoactivator production immediately after stimulation, achieving these levels of fold-change induction is likely difficult for $d \geqslant 2$. However, whether this is actually the scenario for the TNF pathway is difficult to say, as this pathway contains important complexities that are outside of our model.

We suggest that there are two key elements lacking in our model that constitute natural next steps for this work and will help make contact with pathways like TNF. First is the extension to time-dependent stimuli. Especially in the context of action potentials in neurons, there is a long history of studying the wave ignition threshold as a function of stimuli that are localized in time as well as space [21]. Such time dependence is equally important to consider for cell signaling responses, which are often dealing with dynamic signals [33]. Extending our analysis to time-dependent stimuli will be an important direction for future work. Second is the addition of negative feedback to the model. In the context of action potentials, negative feedback is a key part of the celebrated Fitz-Hugh Nagumo model and generates complex behaviors including oscillations [20,21]. In the context of cell signaling, negative feedback is also widespread, including in the TNF pathway, where it produces oscillations of the transcription factor NF-κB in and out of the nucleus [11,12,33,42]. Negative feedback was also found to be important for tuning the bistability of a programed cell death signaling network that supports trigger waves [10]. It would be interesting to see if the scaling behavior of our results derived here holds with the addition of negative feedback.

ACKNOWLEDGMENTS

B.H.S., W.S.D., and K.S. were funded by individual fellowships from the James S. McDonnell Foundation (Grants No. 2020-1172, No. 2021-3227, and No. 2021-3208, respectively). Y.Z. was supported by an Omidyar Fellowship from the Santa Fe Institute. In addition, we gratefully acknowledge the James S. McDonnell Foundation and the Santa Fe Institute for supporting this work through funding for two working groups held at the Santa Fe Institute in March and October 2023. We thank Isa Stallworthy and Hana Mir for helpful discussions, Yasemin Kirişçioğlu for help tracking down the Mornev reference [15], and Hilary Skolnik, Bruce Bertram, and Jen Leighton for logistical support at the Santa Fe Institute.

DATA AVAILABILITY

The data that support the findings of this article are openly available [43].

APPENDIX A: DERIVING A CONTINUUM MODEL OF IMMUNE TRIGGER WAVES

Consider a one-dimensional lattice of cells of size l_{cell} indexed by position i that produce an autoactivator u in response to a stimulus $2I$ at the origin and in response to itself,

$$\dot{u}_i = k\frac{u_i^n}{K_D^n + u_i^n} - \gamma u_i + 2I\delta_{i,0} + \frac{1}{\tau}(u_{i+1} + u_{i-1} - 2u_i), \tag{A1}$$

with τ the timescale of molecules of u hopping between lattice sites. On taking the continuum limit, we obtain

$$\partial_t u = D\partial_x^2 u + k\frac{u^n}{K_D^n + u^n} - \gamma u + 2\, l_{\text{cell}}\, I\, \delta(x), \tag{A2}$$

where $u(x, t)$ is a continuous field and the diffusion coefficient $D \equiv l_{\text{cell}}^2/\tau$. The factor of l_{cell} in the stimulus term comes from turning the Kronecker delta into the Dirac delta function in the continuum limit. In d spatial dimensions, the δ function acquires a prefactor of $(l_{\text{cell}})^d$, as is required by dimensional analysis.

APPENDIX B: WELL-MIXED ANALYSIS

For analyzing the behavior of a well-mixed population of cells, we consider the following ordinary differential equation, which contains only the reaction terms of the reaction-diffusion model in Eq. (2):

$$\dot{u} = \frac{u^n}{K_D^n + u^n} - u + 2I, \quad u(0) = 0. \tag{B1}$$

As explained in the main text (Sec. II A), (B1) permits three fixed points: one unstable and two stable, where the stable node of lower value is termed the "low" state and of higher value the "high" state. We seek the critical value $I = I_c^{\text{mixed}}$, that drives u to its high state. Since we always have the initial condition $u(0) = 0$, we can simply ask what value of I causes us to lose the low stable fixed point, forcing the system to flow to the high fixed point. As in the main text, we work in the "high-sensitivity" limit $K_D \ll 1$.

Setting $\dot{u} = 0$, we get the polynomial

$$-u^{n+1} + (1 + 2I)u^n - K_D^n u + 2IK_D^n = 0. \tag{B2}$$

To identify when this system loses its low stable fixed point, we must compute the value of I that causes this polynomial to go from three to two unique positive real roots, due to the lowest two roots merging. In the main text Sec. II A, we show that the second largest root is approximated by $K_D^{n/(n-1)}$ for $K_D \ll 1$. Since $K_D^{n/(n-1)}$ will also be small when K_D is small, we can simplify the problem by dropping the highest power in u. Rearranging a bit, we have

$$u^n - \frac{K_D^n}{1+2I}u + \frac{2IK_D^n}{1+2I} = 0. \tag{B3}$$

So now we want to know when this polynomial goes from having two unique positive real roots to one.

Applying Descarte's rule of signs [44], (B3) has either two or zero positive real roots. Therefore, we are looking for when the two roots become degenerate. A polynomial will have degenerate roots when its discriminant is zero. While computing discriminants for general n-degree polynomials is intractable, our trinomial form (B3) has an explicit expression for the discriminant.

Theorem 1 from Ref. [35] states that for a general trinomial

$$x^n + c_1 x^k + c_2, \tag{B4}$$

the discriminant is given by

$$D_f = n^n(-1)^{\frac{n(n-1)}{2}} c_2^{k-1} \times \left[c_2^{\frac{n-k}{d}} - (-1)^{\frac{n}{d}} c_1^{\frac{n}{d}} \left(1 - \frac{k}{n}\right)^{\frac{n-k}{d}} \left(\frac{k}{n}\right)^{\frac{k}{d}} \right]^d, \tag{B5}$$

where $d \equiv \gcd(n, k)$. In our case, $k = 1$, so $d = \gcd(n, 1) = 1$ and $c_1 < 0$. The term in brackets determines when $D_f = 0$, which simplifies to [with $c_1 \to -c_1$ for notational consistency with (B3)]

$$c_2 = c_1^{\frac{n}{n-1}} \left(1 - \frac{1}{n}\right)\left(\frac{1}{n}\right)^{\frac{1}{n-1}}. \tag{B6}$$

Substituting for c_1 and c_2 from (B3), we get

$$2I(1+2I)^{\frac{1}{n-1}} = \left(1 - \frac{1}{n}\right)\left(\frac{1}{n}\right)^{\frac{1}{n-1}} K_D^{\frac{n}{n-1}}. \tag{B7}$$

Dropping the $(1 + 2I)$ term, we arrive at the critical well-mixed activation threshold,

$$I_c^{\text{mixed}} = \frac{1}{2}\left(1 - \frac{1}{n}\right)\left(\frac{1}{n}\right)^{\frac{1}{n-1}} K_D^{\frac{n}{n-1}}. \tag{B8}$$

Restoring dimensional units, we get the final result,

$$I_c^{\text{mixed}} = \frac{1}{2}\left(1 - \frac{1}{n}\right)\left(\frac{1}{n}\right)^{\frac{1}{n-1}} \left(\frac{K_D}{k/\gamma}\right)^{\frac{n}{n-1}} k. \tag{B9}$$

Higher-order contributions to I_c^{mixed} can be calculated; we do not pursue this here, as the leading-order result appears quite accurate [see Figs. 2(e)–2(g) of the main text].

APPENDIX C: TRIGGER WAVE IGNITION THRESHOLD

The nondimensionalized model in $d = 1$ reads

$$\partial_t u = \partial_x^2 u + f(u) + 2I\,\delta(x), \tag{C1}$$

with

$$f(u) = \frac{u^n}{K_D^n + u^n} - u \tag{C2}$$

(for simplicity, we absorb the factor of l_{cell} into our definition of I). Our goal is to calculate the critical value of I that ignites a trigger wave. We follow the result of Mornev [15], mentioned more recently in Ref. [21] and also related to approaches outlined in Ref. [36]. This result says that, for any bistable $f(u)$ with three fixed points, $u_1 < u_2 < u_3$, the critical value of I is given by

$$I_c^{\text{wave}} = \left(-2\int_{u_1}^{u_2} f(u)\,du\right)^{1/2}. \tag{C3}$$

We derived the fixed points u_1 and u_2 in the main text Sec. II A ($u_1 = 0$, $u_2 \approx K_D^{n/(n-1)}$) and will compute the integral below. Before proceeding with the calculation, however, we give a brief sketch of the derivation. Mornev's original work is in Russian, which none of the present authors can read. Therefore, we give here our own derivation of Eq. (C3), which we believe is related to the original paper.

1. Deriving Mornev's result

The idea of this approach to is to study when steady-state solutions of Eq. (C1) that decay to zero cease to exist. In the steady state, we have

$$u'' = -f(u) - 2I\delta(x). \tag{C4}$$

We approach the analysis by rewriting this equation as two first-order equations,

$$u' = v, \tag{C5}$$

$$v' = -f(u), \tag{C6}$$

and replacing the delta function stimulus with a boundary condition on $v(x)$ at $x = 0$. This system exhibits a constant of motion, or "energy," given by

$$E = \frac{v^2}{2} + U(u) \tag{C7}$$

with potential function

$$U(u) = \int_0^u ds f(s). \tag{C8}$$

Here "constant of motion" means a function that is constant along the profile of the solution in space. Therefore, we can construct solutions with particular energy values using the relation

$$u' = \sqrt{2(E - U(u))}. \tag{C9}$$

We are only interested in solutions with zero flux at $x \to \pm\infty$. For solutions that decay to zero at $x \to \pm\infty$, in the u-u' plane the solution sets asymptotically approach $(u, u') = (0, 0)$ (Fig. 3). Since $U(0) = 0$, the only value of E that contains $(u, u') = (0, 0)$ is $E = 0$. Thus, we conclude that steady-state solutions that decay to zero are defined by the

relation

$$u' = \sqrt{-2\int f(u)du}. \tag{C10}$$

In Fig. 3(b) of the main text, we plot this solution set in the u'-u plane as a solid gray curve. It consists of a closed curve that starts and ends at $(u, u') = (0, 0)$ (a homoclinic orbit). In a similar way, we can find the set that corresponds to solutions that contain $(u, u') = (u_3, 0)$, which correspond to solutions with uniform high activity [u_3 being the high fixed point of $f(u)$]. This solution corresponds to $E = \int_0^{u_3} f(u)du$. We plot this solution set in Fig. 3(b) as a solid cyan curve. Finally, since the delta function stimulus term enforces a boundary condition on $u'(0)$, it can be drawn as horizontal lines in the u-u' plane [dashed black lines in Fig. 3(b)].

By visual inspection, we see that for a critical value of the stimulus strength, I, the horizontal lines representing the boundary condition will lift off of the gray solution set corresponding to decaying solutions, leaving only the uniform high-state solution in cyan being a possibility. This transition corresponds to the onset of trigger waves. The transition point can be computed since it is the apex of the decaying solution curve, so occurs at the maximum of the function Eq. (C10). Differentiating Eq. (C10) once, we recover the fact that $u'' = -f(u)$, and so observe that the apex of the curve occurs at $u = u_2$. Evaluating $u'(u_2)$, we arrive at the critical gradient at the origin,

$$(u')_c = \sqrt{-2\int_{u_1}^{u_2} f(u)du}. \tag{C11}$$

The last piece is to note that having a stimulus strength of $2I$ creates a gradient at $x = 0$ of magnitude I on either side of the origin (hence the factor of 2 in the definition of I). To see this, consider integrating the steady state of Eq. (C1) across a small region $(-\Delta, \Delta)$ around the origin and taking the limit $\Delta \to 0$. The reaction term $f(u)$ is continuous across the origin, so does not contribute. We are left with a jump condition on the gradient:

$$u'(0^+) - u'(0^-) = -2I, \tag{C12}$$

where $0^\pm$ represents the limit of $x \to 0$ from either the right or the left. By symmetry, $u'(0^+) = -u'(0^-)$, so we have on each side of the origin a gradient with magnitude I. With this last piece, we arrive at Mornev's result Eq. (C3).

2. Computing the integral in (C3)

For the integral

$$\int_0^{K_D^{n/(n-1)}} du\left(\frac{u^n}{K_D^n + u^n} - u\right), \tag{C13}$$

since $K_D^{n/(n-1)} \ll K_D$ for $K_D \ll 1$, we can approximate the integrand of the first term by its small-u behavior (as u is only being integrated up to a small number) and find

$$\int du \frac{u^n}{K_D^n + u^n} \approx \frac{K_D^{-n} u^{n+1}}{n+1}. \tag{C14}$$

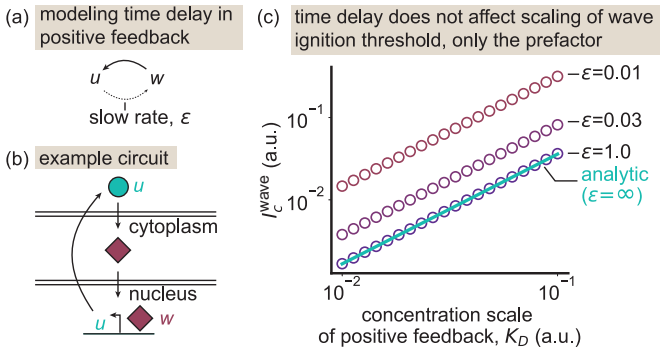

FIG. 5. Time delay in the positive feedback does not impact the scaling of the trigger wave threshold with K_D. (a) Schematic of the model. The positive feedback loop in u activation is mediated through a slow intermediate, w. The time delay is controlled by the dimensionless rate, ϵ. (b) Example signaling network that implements the model. The secreted signal, u, induces the nuclear localization of a transcription factor, w, which in turn activates production of u. (c) Numerical results for the trigger wave threshold in 1D for various values of ϵ. The analytic result for the model with only u (cyan line), which corresponds to $\epsilon \to \infty$, agrees well with simulations down to $\epsilon \approx 1$. For smaller ϵ, the scaling with K_D remains unchanged, but the prefactor grows. In these simulations, the Hill coefficient was $n = 4$.

Including the linear term from (C13), we obtain

$$\int_0^{K_D^{n/(n-1)}} du\left(\frac{u^n}{K_D^n + u^n} - u\right) = \frac{1}{n+1}K_D^{\frac{2n}{n-1}} - \frac{1}{2}K_D^{\frac{2n}{n-1}} = \left(\frac{1}{n+1} - \frac{1}{2}\right)K_D^{\frac{2n}{n-1}}. \tag{C15}$$

Substituting into (C3), we get

$$I_c^{\text{wave}} = \left(\frac{n-1}{n+1}\right)^{1/2} K_D^{\frac{n}{n-1}}, \tag{C16}$$

and converting to dimensional form, we have

$$I_c^{\text{wave}} = \left(\frac{n-1}{n+1}\right)^{1/2}\left(\frac{K_D}{k/\gamma}\right)^{\frac{n}{n-1}}\sqrt{\frac{D}{\gamma}}\,k. \tag{C17}$$

APPENDIX D: MODEL WITH TIME DELAY

Real cell signaling networks exhibit time delays that can qualitatively affect the resulting dynamics. To assess the impact of such a delay on the scaling behavior of the trigger wave ignition threshold, we extended the model in Eq. (C1) to include an intermediate signaling molecule, $w(x, t)$. We assume that w is not secreted but only functions inside each cell as a rate-limiting step of the autoactivation circuit [Figs. 5(a) and 5(b)]. The extended model is

$$\begin{aligned}\partial_t u &= D\nabla^2 u + k_u\frac{w^n}{K_D^n + w^n} - \gamma_u u + 2(l_{\text{cell}})^d I\delta(x)\\ \partial_t w &= k_w u - \gamma_w w,\end{aligned} \tag{D1}$$

where we have introduced distinct production and loss rates for u and w. We nondimensionalize this model in a

similar manner to the original: $t \to \gamma_u t$, $x \to x/\sqrt{D/\gamma_u}$, $u \to u/(k_u/\gamma_u)$, and new for this model, $w \to w/(k_w k_u/\gamma_w \gamma_u)$. With these choices, the model in dimensionless form reads

$$\begin{aligned} \partial_t u &= \nabla^2 u + \frac{w^n}{K_D^n + w^n} - u + 2(l_{\text{cell}})^d I\delta(x) \\ \partial_t w &= \epsilon(u - w), \end{aligned} \tag{D2}$$

with $\epsilon \equiv \gamma_w/\gamma_u$ setting the timescale separation between u and w dynamics and K_D and l_{cell} now rescaled accordingly.

We numerically tested how the time delay, encoded by the dimensionless parameter ϵ, alters the scaling of the trigger wave ignition threshold, I_c^{wave}. We found that I_c^{wave} followed the $K_D^{n/(n-1)}$ scaling of the u-only model for all values of ϵ tested [Fig. 5(c)]. Only the prefactor was affected. Our analytic result, which corresponds to the limit $\epsilon \to \infty$, such that $w = u$, agrees well with simulations down to $\epsilon \approx 1$. Therefore, we conclude that our results for a simplified, one variable model [Eq. (C1)] can be used to understand the qualitative behavior of more complicated models that include a time delay in autoactivation.

APPENDIX E: RELATION TO A CUBIC MODEL

In this Appendix, we elaborate on the relationship between the Hill function model studied in this paper and the more popular cubic activation model,

$$\partial_t u = \partial_x^2 u + f_3(u) + 2I\delta(x), \tag{E1}$$

with

$$f_3 = u(u-\theta)(1-u) = -u^3 + (1+\theta)u^2 - \theta u. \tag{E2}$$

This model is sometimes called the Nagumo equation, being the fast subsystem of the FitzHugh-Nagumo equation. Its ignition criteria was studied in detail in Ref. [19], including time-dependent stimuli. The parameter θ sets the threshold of the positive feedback, so it plays a role analogous to K_D in the Hill function model.

We briefly sketch out a calculation of activation thresholds for the cubic model here. Recall that the starting point is to identify u_2, the intermediate root of the activation function. The factorized form of $f_3(u)$ allows us to trivially read off that $u_2 = \theta$ (this factorized form also guarantees bistability for all values of θ, unlike the Hill function model, which can become monostable for large K_D). To find the well-mixed activation threshold, we compute when the function

$$-u^3 + (1+\theta)u^2 - \theta u + 2I = 0 \tag{E3}$$

goes from having three to two roots. Since our goal here is simply to compare the scaling behavior of this model with the Hill function model, we work in the $\theta \ll 1$ limit, which allows us to simplify by dropping the cubic term. We then solve for when the discriminant of the resulting quadratic polynomial is equation zero, finding

$$I_c^{\text{mixed}} \approx \frac{\theta^2}{8}. \tag{E4}$$

To find the trigger wave ignition threshold, we compute the integral in Eq. (C3) and find that

$$I_c^{\text{wave}} = \frac{\theta^{3/2}}{\sqrt{3}}. \tag{E5}$$

Notably, the well-mixed and wave activation thresholds scale differently with the threshold parameter θ—the former scaling as θ^2, the latter as $\theta^{3/2}$—whereas in the Hill function model, both scale as $K_D^{n/(n-1)}$.

To understand this qualitative difference between cubic and Hill function models, we can construct a Hill function model that is close in spirit to the cubic model. Since we work in the limit of $K_D \ll 1$, and we found that $u_2 \approx K_D^{n/(n-1)} \ll K_D$ for small K_D, we can approximate the Hill function by an appropriate polynomial:

$$f(u) = \frac{u^n}{K_D^n + u^n} - u \approx \left(\frac{u}{K_D}\right)^n - \left(\frac{u}{K_D}\right)^{2n} - u. \tag{E6}$$

For $n = 2$, this function becomes

$$f(u) \approx \left(\frac{u}{K_D}\right)^2 - \left(\frac{u}{K_D}\right)^4 - u, \tag{E7}$$

which resembles the cubic model, but with a u^4 saturating term instead of u^3 (recall from our calculations above that the large u behavior of the activation function, governed here by the u^4 term and by the u^3 term in the cubic model, is unimportant for the threshold behavior; the important feature to match is the u^2 term that governs the nonlinear positive feedback). To compare directly with the cubic model, we can rewrite this equation as

$$f(u) \approx \frac{1}{K_D^2}\left(-\frac{1}{K_D^2}u^4 + u^2 - K_D^2 u\right). \tag{E8}$$

Then, we redefine $\theta \equiv K_D^2$. Comparing to Eq. (E2), we see that to leading order in θ the Hill model with $n = 2$ resembles the cubic model with an overall prefactor of $1/\theta$:

$$f(u) \approx \frac{1}{\theta}\left(-\frac{1}{\theta}u^4 + u^2 - \theta u\right). \tag{E9}$$

This mapping between models tells us that to understand the different scaling behaviors in the Hill function and cubic models, we need to understand how the well-mixed and wave activation thresholds behave when the function $f_3(u)$ is scaled by a factor of $1/\theta$. The well-mixed threshold is determined by the discriminant of the polynomial in (E3). Working to quadratic order in u, let us write the activation function (E2) in general terms as

$$f_3(u) \approx au^2 - bu. \tag{E10}$$

Under a scaling transformation $f_3(u) \to (1/\theta)f_3(u)$, the coefficients a and b are both scaled by $1/\theta$. The discriminant of the polynomial

$$au^2 - bu + 2I \tag{E11}$$

is

$$\Delta = b^2 - 8aI. \tag{E12}$$

As above, the well-mixed activation threshold is the value of I such that $\Delta = 0$ or

$$I_c^{\text{mixed}} = \frac{b^2}{8a}. \tag{E13}$$

Under the scaling transformation

$$f_3(u) \to (1/\theta) f_3(u), \tag{E14}$$

I_c^{mixed} therefore also transforms as

$$I_c^{\text{mixed}} \to (1/\theta) I_c^{\text{mixed}}. \tag{E15}$$

In the cubic model, $I_c^{\text{mixed}} \sim \theta^2$. So, for the Hill function model, which we deduced corresponds in essence to the cubic model with $f_3(u) \to (1/\theta) f_3(u)$, we expect

$$I_c^{\text{mixed}} \sim \theta \sim K_D^2, \tag{E16}$$

agreeing with our result of $I_c^{\text{mixed}} \sim K_D^{n/(n-1)}$ with $n = 2$.

Now we consider the wave activation threshold. We previously showed that

$$I_c^{\text{wave}} \sim \left(- \int_0^{u_2} du\, f(u) \right)^{1/2} \tag{E17}$$

[Equation (C3)]. So, under the scaling transformation $f_3(u) \to (1/\theta) f_3(u)$, the wave activation threshold transforms as

$$I_c^{\text{wave}} \to \theta^{-1/2} I_c^{\text{wave}}. \tag{E18}$$

For the cubic model we have $I_c^{\text{wave}} \sim \theta^{3/2}$, so for the Hill function model we expect

$$I_c^{\text{wave}} \sim \theta \sim K_D^2, \tag{E19}$$

agreeing with our result of $I_c^{\text{wave}} \sim K_D^{n/(n-1)}$ with $n = 2$.

Through this analysis, we see that the difference in scaling behavior of activation thresholds between the cubic and Hill function models arises from how the threshold parameter (θ for the cubic model and K_D for the Hill model) enters the activation function. Aside from this parametrization difference, the models are qualitatively very similar in their activation behavior.

APPENDIX F: NUMERICAL SCHEME

We solved the PDE Eq. (C1) using the Crank-Nicolson method with an adaptive timestep implemented in Python, building on the `diffrax` package [45]. Our simulation code, along with code for reproducing the figures of this paper, is available [43]. For the PDE, we approximated the Dirac delta function using a Gaussian of width equal to half of the grid spacing. For the ODE model, we used the same solver but had a grid with a single grid point. For our verification of the scaling predictions from dimensional analysis (Fig. 6), we directly solved the dimensionful model [Eq. (A2)].

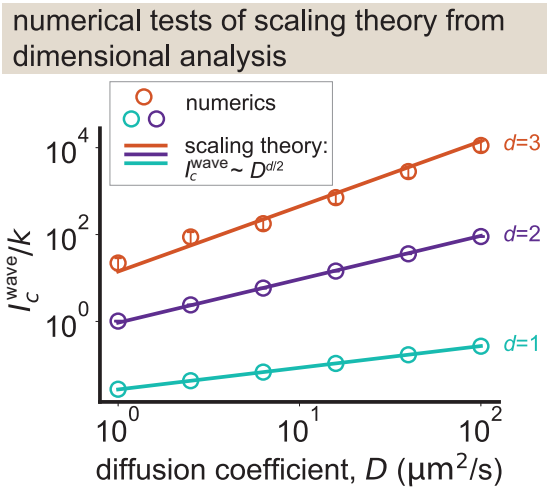

FIG. 6. Verifying scaling theory predictions based on dimensional analysis through dimensionful numerics. Circles are numerical results for I_c^{wave}/k versus the diffusion coefficient, D, computed using the dimensionful model Eq. (A2). Here k is the production rate associated with positive feedback, so the ratio I_c^{wave}/k is dimensionless and expresses the ratio of the production of the autoactivator that comes from the external stimulus versus from positive feedback. Lines are the predictions of dimensional analysis, $I_c^{\text{wave}} \sim D^{d/2}$. We fit the intercept of a line with slope $d/2$ to the log-transformed quantities. Error bars represent the final bounds of our binary search optimization algorithm for empirically finding the value of I that leads to wave ignition (e.g., the true critical value lies within the error bars). Parameters: $n = 4$, $\gamma = 0.23$/min, $k = 1$ a.u./min, and $K_D/(k/\gamma) = 0.01$ a.u.

To numerically determine the activation thresholds in simulations, we performed binary search. For a given stimulus strength, we integrate the model to a steady state, which is considered activated (unactivated) if mean u over the spatial domain is greater (less) than 0.5. We initialize with lower and upper bounds for the critical stimulus, first checking their steady states, and extended the bounds if necessary. Then we evaluate activation using stimulus strength at the midpoint of the bounding interval. If this midpoint results in an activated (unactivated) steady state, then it becomes the new upper (lower) bound. This step is iterated until the size of the bounding interval is below a tolerance, and the midpoint is taken as the estimated activation threshold. Error bars for the activation threshold are then given by the lower and upper bounds at the final iteration. Simulations were run on a custom-built computer with an Intel Core i9 11900K processor and 128 GB RAM running Ubuntu 20.04.

[1] B. Alberts, R. Heald, A. Johnson, D. Morgan, M. Raff, K. Roberts, and P. Walter, *Molecular Biology of the Cell (Seventh Edition)* (W. W. Norton, New York, 2022).

[2] A. Einstein, Über die von der molekularkinetischen Theorie der Wärme geforderte Bewegung von in ruhenden Flüssigkeiten suspendierten Teilchen, Ann. Phys. **322**, 549 (1905).

[3] R. Phillips, J. Kondev, J. Theriot, and H. Garcia, *Physical Biology of the Cell* (Garland Science, New York, 2012).

[4] L. Gelens, G. A. Anderson, and J. E. Ferrell Jr, Spatial trigger waves: Positive feedback gets you a long way, Mol. Biol. Cell **25**, 3486 (2014).

[5] K Hara, Cinematographic observation of "surface contraction waves" (SCW) during the early cleavage of axolotl eggs, W. Roux' Arch Entwicklungsmech. Org. **167**, 183 (1971).
[6] J. B. Chang and J. E. Ferrell, Jr., Mitotic trigger waves and the spatial coordination of the Xenopus cell cycle, Nature (Lond.) **500**, 603 (2013).
[7] M. Vergassola, V. E. Deneke, and S. Di Talia, Mitotic waves in the early embryogenesis of Drosophila: Bistability traded for speed, Proc. Natl. Acad. Sci. USA **115**, E2165 (2018).
[8] A. H. Cornell-Bell, S. M. Finkbeiner, M. S. Cooper, and S. J. Smith, Glutamate induces calcium waves in cultured astrocytes: long-range glial signaling, Science, **247**, 470 (1990).
[9] Y. Fan, C. Chai, P. Li, X. Zou, J. E. Ferrell, Jr., and B. Wang, Ultrafast distant wound response is essential for whole-body regeneration, Cell **186**, 3606 (2023).
[10] H. K. C. Co, C.-C. Wu, Y.-C. Lee, and Sheng-hong Chen, Emergence of large-scale cell death through ferroptotic trigger waves, Nature (London) **631**, 654 (2024).
[11] P. Yde, M. Hogh Jensen, and A. Trusina, Analyzing inflammatory response as excitable media, Phys. Rev. E **84**, 051913 (2011).
[12] P. Yde, B. Mengel, M. H. Jensen, S. Krishna, and A. Trusina, Modeling the NF-κB mediated inflammatory response predicts cytokine waves in tissue, BMC Syst. Biol. **5**, 115 (2011).
[13] R Luther, Räumliche Fortpflanzung chemischer Reaktionen, Z. Elektrochem. Angew. Phys. Chem. **12**, 596 (1906).
[14] C. Trentesaux, T. Yamada, O. D. Klein, and W. A. Lim, Harnessing synthetic biology to engineer organoids and tissues, Cell Stem Cell **30**, 10 (2023).
[15] O. A. Mornev, *On the Conditions of Excitation of One-dimensional Autowave Media: Autowave Processes in Systems with Diffusion* (Institute of Applied Physics of the USSR Academy of Sciences, Gorky, 1981), pp. 92–98.
[16] H. P. McKean and V. Moll, A threshold for a caricature of the nerve equation, Bull. Am. Math. Soc. **12**, 255 (1985).
[17] G. Flores, The stable manifold of the standing wave of the Nagumo equation, J. Diff. Equ. **80**, 306 (1989).
[18] J. C. Neu, R. S. Preissig, and W. Krassowska, Initiation of propagation in a one-dimensional excitable medium, Physica D **102**, 285 (1997).
[19] I. Idris and V. N. Biktashev, Analytical approach to initiation of propagating fronts, Phys. Rev. Lett. **101**, 244101 (2008).
[20] B. Bezekci and V. N. Biktashev, Fast-slow asymptotic for semi-analytical ignition criteria in FitzHugh-Nagumo system, Chaos **27**, 093916 (2017).
[21] B. Bezekci and V. N. Biktashev, Strength-Duration relationship in an excitable medium, Commun. Nonlin. Sci. Numer. Simul. **80**, 104954 (2020).
[22] J. Zhao, M. L. Perkins, M. Norstad, and H. G. Garcia, A bistable autoregulatory module in the developing embryo commits cells to binary expression fates, Curr. Biol. **33**, 2851 (2023).
[23] H. Tran, J. Desponds, C. A. P. Romero, M. Coppey, C. Fradin, N. Dostatni, and A. M. Walczak, Precision in a rush: Trade-offs between reproducibility and steepness of the hunchback expression pattern, PLoS Comput. Biol. **14**, e1006513 (2018).
[24] G. Birzu, O. Hallatschek, and K. S. Korolev, Fluctuations uncover a distinct class of traveling waves, Proc. Natl. Acad. Sci. USA **115**, E3645 (2018).
[25] W. van Saarloos, Front propagation into unstable states, Phys. Rep. **386**, 29 (2003).
[26] M. O. Lavrentovich and D. R. Nelson, Asymmetric mutualism in two- and three-dimensional range eExpansions, Phys. Rev. Lett. **112**, 138102 (2014).
[27] M. Gralka and O. Hallatschek, Environmental heterogeneity can tip the population genetics of range expansions, eLife **8**, e44359 (2019).
[28] S. R. Gandhi, E. A. Yurtsev, K. S. Korolev, and J. Gore, Range expansions transition from pulled to pushed waves as growth becomes more cooperative in an experimental microbial population, Proc. Natl. Acad. Sci. USA **113**, 6922 (2016).
[29] V. Volpert and S. Petrovskii, Reaction-diffusion waves in biology: New trends, recent developments, Phys. Life Rev. **52**, 1 (2025).
[30] A. M. Turing, The chemical basis of morphogenesis, Philos. Trans. R. Soc. Lond. B **237**, 37 (1952).
[31] R. A. Fisher, The wave of advance of advantageous genes, Ann. Eugenics **7**, 355 (1937).
[32] A. Kolmogorov, I. Petrovskii, and N. Piskunov, A study of the diffusion equation with increase in the amount of substance, and its application to a biological problem, Mosc. Univ. Math. Bull. **1**, 1 (1937).
[33] M. Son, T. Frank, T. Holst-Hansen, A. G. Wang, M. Junkin, S. S. Kashaf, A. Trusina, and S. Tay, Spatiotemporal NF-κB dynamics encodes the position, amplitude, and duration of local immune inputs, Sci. Adv. **8**, eabn6240 (2022).
[34] C. Sokolik, Y. Liu, D. Bauer, J. McPherson, M. Broeker, G. Heimberg, L. S. Qi, D. A. Sivak, and Matt Thomson, Transcription factor competition allows embryonic stem cells to distinguish authentic sSignals from noise, Cell Syst. **1**, 117 (2015).
[35] R. Swan, Factorization of polynomials over finite fields, Pacific J. Math. **12**, 1099 (1962).
[36] V. Arnold, *Ordinary Differential Equations* (MIT Press, Cambridge, MA, 1973).
[37] L. J. M. Bruurs, M. Müller, J. G. Schipper, H. H. Rabouw, S. Boersma, F. J. M. van Kuppeveld, and M. E. Tanenbaum, Antiviral responses are shaped by heterogeneity in viral replication dynamics, Nat. Microbiol. **8**, 2115 (2023).
[38] R. A. Gottschalk, A. J. Martins, B. R. Angermann, B. Dutta, C. E. Ng, S. Uderhardt, J. S. Tsang, I. D. C. Fraser, M. Meier-Schellersheim, and R. N. Germain, Distinct NF-κB and MAPK activation thresholds uncouple steady-state microbe sensing from anti-pathogen inflammatory responses, Cell Syst. **2**, 378 (2016).
[39] R. Singh, S. Harsh, A. Bajpai, S. Pal, R. K. Pandey, and P. Sinha, A Serpin27A-dependent Toll signaling underlies host genetics of cancer resistance in *Drosophila*, bioRxiv [Preprint] (2021), doi:10.1101/2021.03.13.435228.
[40] G. Zahn and A. Greischel, Pharmacokinetics of tumor necrosis factor alpha after intravenous administration in rats. Dose dependence and influence of tumor necrosis factor beta, Arzneimittel-Forsch. **39**, 1180 (1989).
[41] T. Moritz, N. Niederle, J. Baumann, D. May, E. Kurschel, R. Osieka, J. Kempeni, E. Schlick, and C. G. Schmidt, Phase I study of recombinant human tumor necrosis factor alpha in advanced malignant disease, Cancer Immunol. Immunother. CII **29**, 144 (1989).
[42] A. Adelaja, B. Taylor, K. M. Sheu, Y. Liu, S. Luecke, and A. Hoffmann, Six distinct NFκB signaling codons

convey discrete information to distinguish stimuli and enable appropriate macrophage responses, Immunity **54**, 916 (2021).

[43] W. S. DeWitt, immunowave (2026), https://github.com/dewitt-lab/immunowave

[44] R. Descartes and I. Maclean, A, *Discourse on the Method, Oxford World's Classics* (Oxford University Press, Oxford, 2006).

[45] P. Kidger, On neural differential equations, Ph.D. thesis, University of Oxford, 2021.